

Effect of Grain Size on the Superplastic Behavior of a 7475 Aluminum Alloy

R.K. Mahidhara

Specimens of a superplastic 7475 aluminum alloy with grain sizes ranging between 9 and 35 μm were tensile tested at a strain rate of $1 \times 10^{-4}/\text{s}$ at 457 and 517 $^{\circ}\text{C}$. At 517 $^{\circ}\text{C}$, the ductility was found to decrease with an increase in grain size. At 457 $^{\circ}\text{C}$, on the other hand, the ductility was found to increase initially and then decrease for grain sizes larger than 14 μm . The latter decrease in ductility is attributed to the lowered ability for grain-boundary sliding with decreasing grain-boundary area. In the as-received material (grain size of 9 μm), the observed low ductility is attributed to an inhomogeneous microstructure.

Keywords

grain-size effects, superplasticity, type 7475 aluminum alloy

1. Introduction

MICROGRAIN superplastic flow generally occurs at relatively low flow stress and results in high tensile ductility with little internal cavitation (Ref 1, 2). The high-temperature deformation of micrograined superplasticity materials over a wide range of strain rates reveals three distinct regions in the log stress (σ) versus log strain rate ($\dot{\epsilon}$) plot. In such a sigmoidal plot, the important regimes are termed region I, region II, and region III. The slope of the curve is the strain-rate sensitivity, m . The strain-rate sensitivity is maximum in the intermediate strain-rate regime II. Therefore, a relatively slow strain rate (10^{-1} to 10^{-5} s) at a temperature of about $0.5 T_M$ (where T_M is the absolute melting temperature of the alloy) is generally required to attain superplastic flow.

In addition, the alloy should possess a fine grain size, which should remain stable during high-temperature deformation. Recent work by Wert et al. (Ref 3) has indicated that grain refinement in conventional 7000 series Al-Zn-Mg-Cu alloys is possible through thermomechanical treatments and that the grain boundaries can be pinned (or stabilized) by the presence of hard intermetallic particles at the boundaries. While further work has demonstrated the potential of 7475 aluminum as a structural alloy, it is known that this alloy cavitates during superplastic flow (Ref 4). The present work emphasizes the conditions under which optimum superplastic ductility can be achieved with minimal cavitation in a 7475 aluminum alloy.

2. Experimental Method

The material was received in the form of a 2.5 mm thick plate thermomechanically processed (Ref 5) to a fine grain size. A range of grain sizes was obtained by heat treating the alloy at 530 $^{\circ}\text{C}$ in a vacuum for various times ranging from 1 day (grain size of 14 μm) to 3 days (grain size of 35 μm). Note that the reported grain size is the value obtained as the cube root of grain sizes measured on three mutually perpendicular directions.

R.K. Mahidhara, High Performance Materials Inc., Washington University, St. Louis, MO 63130, USA.

The superplasticity of 7475 aluminum alloy was evaluated by performing uniaxial tensile tests. Both differential and constant strain-rate tests were performed on an MTS (MTS Systems Corp., Eden Prairie, MN) machine. Metallography involved optical and transmission electron microscopy (TEM). Density measurements were performed on samples cut from the gage section of the deformed specimens. This was done by hydrostatic weighing in a methyl iodide solution (density of 2.28 g/cm^3 at 21 $^{\circ}\text{C}$), using an electronic balance of ± 0.1 mg sensitivity, with a sample cut from the shoulder of the specimens used as the comparative density standard for each specimen.

3. Experimental Results

The grain growth resulting from annealing the alloy at 530 $^{\circ}\text{C}$ is evident in Fig. 1. Specimens annealed for 1 day at 530 $^{\circ}\text{C}$ (grain size of 14 μm) were used to obtain the stress/strain-rate data shown in Fig. 2. It is evident that a strain rate of $1 \times 10^{-4}/\text{s}$ lies in the superplastic regime (region II). This strain rate was used for all the experimentation reported here.

Figure 3(a) shows the percentage elongation to failure for this alloy as a function of grain size for two different test temperatures. At 517 $^{\circ}\text{C}$, the ductility of the alloy decreases with increasing grain size until a grain size of about 20 μm is reached. Beyond this, no appreciable drop in ductility occurs. At 457 $^{\circ}\text{C}$, on the other hand, the ductility is first seen to increase with grain size. Beyond 14 μm , however, the ductility decreases sharply until about 20 μm . Beyond this, there is again very little effect of grain size.

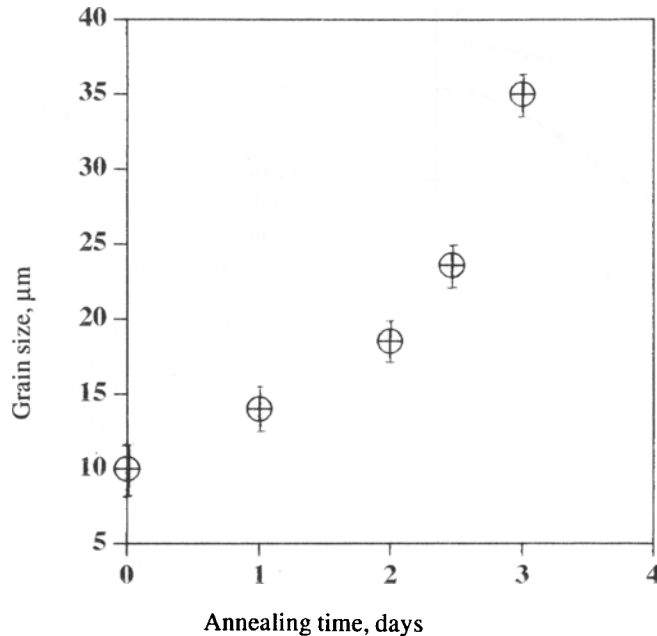
A corresponding plot of percentage cavitation (from density measurements) as a function of grain size is shown in Fig. 3(b). At 517 $^{\circ}\text{C}$, a progressive increase in the level of cavitation occurs as the grain size is increased. At 457 $^{\circ}\text{C}$, on the other hand, a drop in the level of cavitation occurs as the grain size is increased from 9 to 14 μm ; beyond this, an increase in cavitation is evident as the grain size increases. For the as-received material (9 μm), the optical micrographs shown in Fig. 4(a) and (b), taken adjacent to the fracture tips, can be used to compare the cavity morphologies at 457 and 517 $^{\circ}\text{C}$, respectively. The lower-temperature specimen (Fig. 4a) shows a large number of small cavities, whereas at a higher temperature (Fig. 4b) a small number of larger cavities are visible, along with extensive cavity interlinkage.

The overall tensile ductility and the strain homogeneity along the gage section of specimens as a function of test temperature and grain size are compared in Fig. 5 and 6. Figure 5 shows the external appearance of specimens of various initial grain sizes tested at 457 and 517 °C at a strain rate of 1×10^{-4} /s. It is quite evident that the maximum ductility is obtained in the finest-grained material (9 μm) when tested at 517 °C. At 457 °C, however, the specimen with a grain size of 14 μm displays the highest ductility.

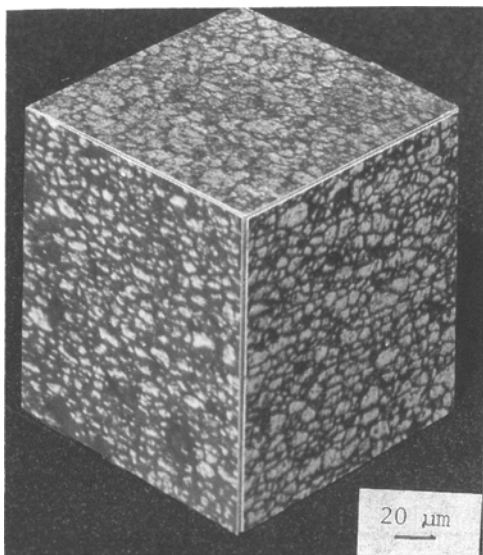
The strain homogeneity along the gage section of these specimens was also monitored by measuring the percentage reduction in area as a function of location along the gage section. The results are shown in Fig. 6(a) and (b) for specimens tested

at 457 and 517 °C, respectively. At the lower test temperature, the largest-grained material shows a sharply localized neck, whereas the others show moderately localized necks. At the higher test temperature, however, all specimens display diffuse necks. The tensile ductility of the 14 μm material was further evaluated over a range of temperatures and strain rates. Some of these results are summarized in Fig. 7(a) and (b). While the steady improvement in ductility with temperature (at a constant strain rate) is seen in Fig. 7(a), the results of Fig. 7(b) show that the ductility as a function of strain rate (at constant temperature) exhibits a maxima at a strain rate of 1×10^{-4} /s.

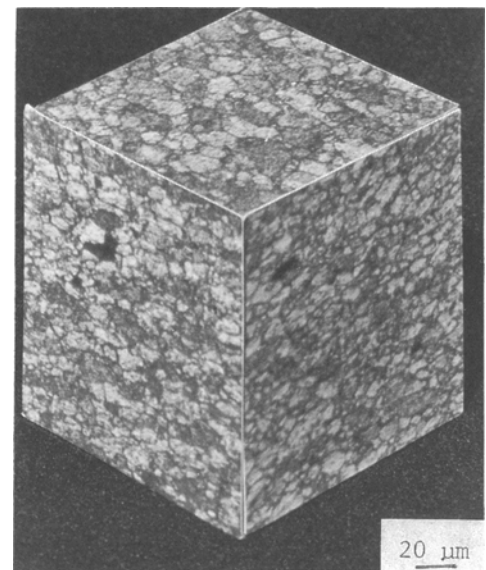
The low ductility (450%) achieved in the as-received (9 μm) material when tested at 457 °C (Fig. 3a) is believed to be asso-



(a)



(b)



(c)

Fig. 1 (a) Plot of grain size versus annealing time. (b and c) Optical micrographs of as-received 7475 Al alloy before (b) and after (c) annealing at 530 °C for 24 h

ciated with the presence of preexisting voids and the ease of decohesion of the small (1.2 μm) particles during grain-boundary sliding (Ref 6). Preexisting voids can arise because many aluminum alloys, including the 7475 alloy, are semicontinuously cast and then chilled in water. It is conceivable that atomic hydrogen thus becomes trapped in the matrix. When this atomic hydrogen recombines to its molecular form, the resulting increase in pressure is presumed to cause the formation of voids. During the preannealing treatment at 530 $^{\circ}\text{C}$ in a vacuum, some of the entrapped gases are outgassed, leading to the collapse of some of these voids. Some voids, however, remain and thus

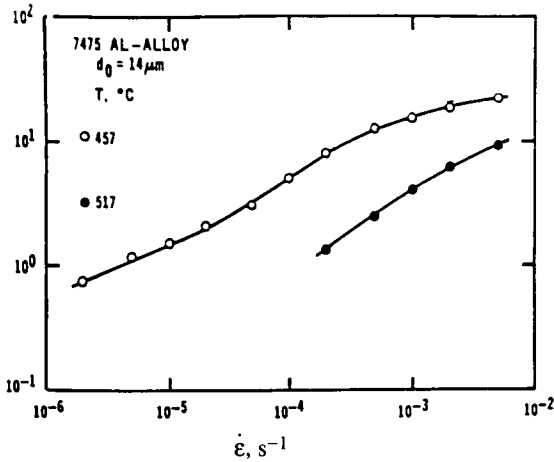


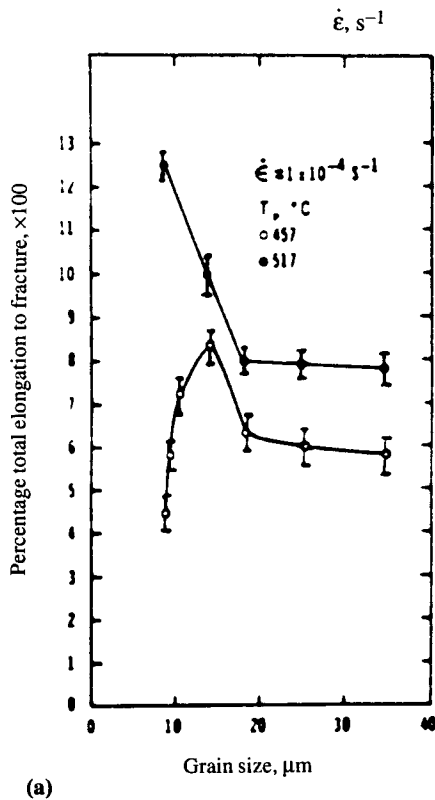
Fig. 2 Log σ versus log $\dot{\epsilon}$ plot for 7475 Al alloy

provide sites for cavity growth during subsequent superplastic deformation. These cavities are in addition to those formed by decohesion of intermetallic particles from the matrix (Ref 7).

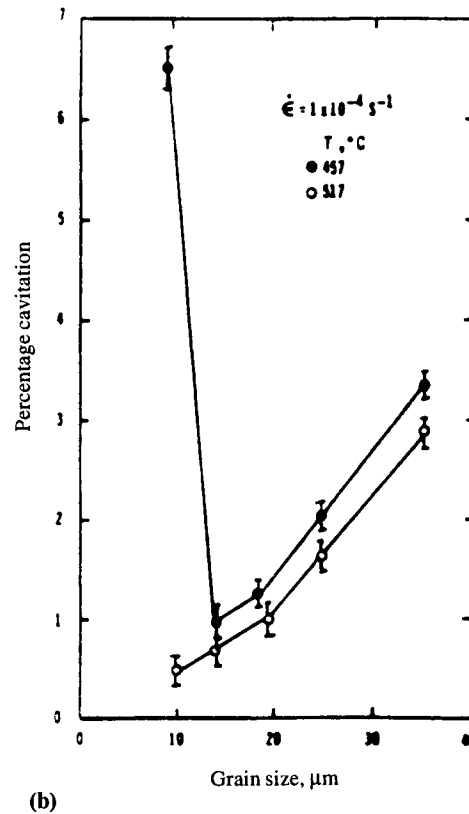
In addition to the outgassing effect, preannealing at 530 $^{\circ}\text{C}$ leads to changes in the size of the intermetallic particles and in grain growth. Particles located in the matrix do not undergo significant size changes, but those located at the grain boundaries do (Ref 8), as observed by TEM. These particles have been found to increase in size from 1.2 to 4.5 μm as a result of preannealing for 24 h. Upon further annealing for 72 and 144 h, the particle size drops to 2.9 and 1.9 μm , respectively, due to dissolution of the intermetallic particles. Grain growth arising from the preannealing leads to an increase in the flow stress and also to reduced grain-boundary sliding ability.

Note, however, that the as-received sample shows a high level of cavitation (Fig. 3b). This implies a high density of rather small cavities. Hence, these cavities need only grow slightly during deformation before they coalesce, leading to premature failure. The rather diffuse necking seen in Fig. 6(a) further supports this. The fact that ductility is controlled by the total volume fraction of voids has also been observed at low strain rates (Ref 9-12).

In the case of specimens annealed for 72 and 144 h at 530 $^{\circ}\text{C}$ (25 and 35 μm grain size, respectively), the low ductility at 457 $^{\circ}\text{C}$ is believed to be associated with the high flow stress and low grain-boundary area in this large-grained condition. Also, if grain-boundary sliding is the operative mechanism, then slip processes must accommodate this sliding. A large grain size corresponds to appreciable distances that dislocations have to

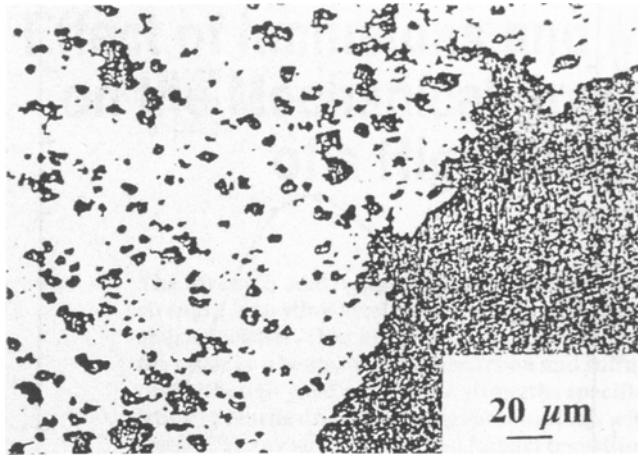


(a)

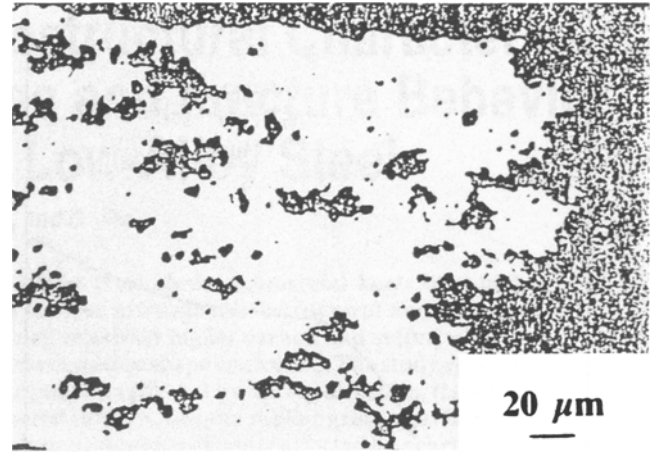


(b)

Fig. 3 Variation of total elongation (a) and percentage cavitation (b) as a function of grain size at 457 and 517 $^{\circ}\text{C}$



(a)



(b)

Fig. 4 Fracture surface of 7475 Al alloy close to the fracture tip at 457 °C (a) and 517 °C (b)

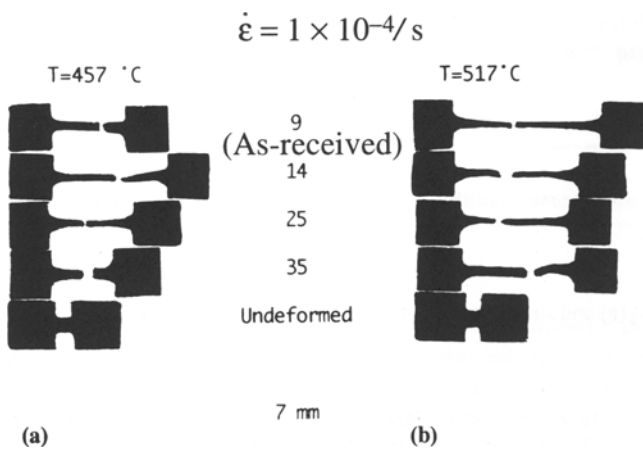


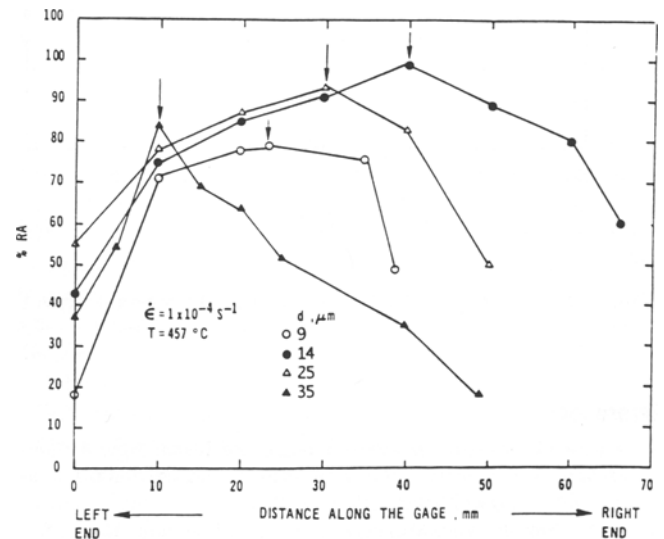
Fig. 5 External appearance of specimens deformed to failure at $T = 457\text{ °C}$ (a) and 517 °C (b) ($\dot{\epsilon} = 1 \times 10^{-4}/s$)

traverse to promote accommodation. Hence, a high level of cavitation is expected; this is indeed seen in Fig. 3(b). It is also seen in Fig. 6(a) that the 25 μm sample shows a rather diffuse neck, whereas the 35 μm sample shows a sharp neck. The latter induces a triaxial state of tensile stress, thereby promoting lateral cavity growth and thus coalescence.

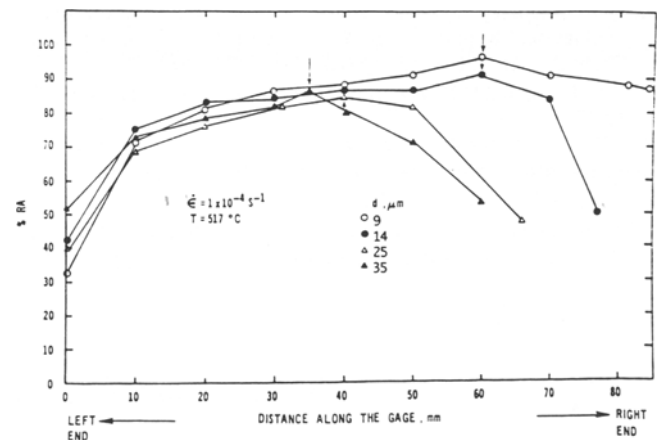
4. Summary and Conclusions

The percentage elongation of the as-received materials was 450 and 1250% at 457 and 517 °C, respectively. Whereas percentage elongation decreases with increasing grain size at 517 °C, at 457 °C it increases to 840% for a grain size of approximately 14 μm and then decreases to 625 and 525%, respectively, for grain sizes of approximately 25 and 35 μm .

Anomalous ductility for the as-received material at 457 °C is attributed to particle matrix decohesion, giving rise to a high nucleation rate of cavities and a concomitant reduced ductility. The decrease in percentage elongation with increasing grain size is attributed to the decreased efficiency of the accommodation process that accompanies grain-boundary sliding at both 457 and 517 °C for specimens with a grain size larger than 14 μm .

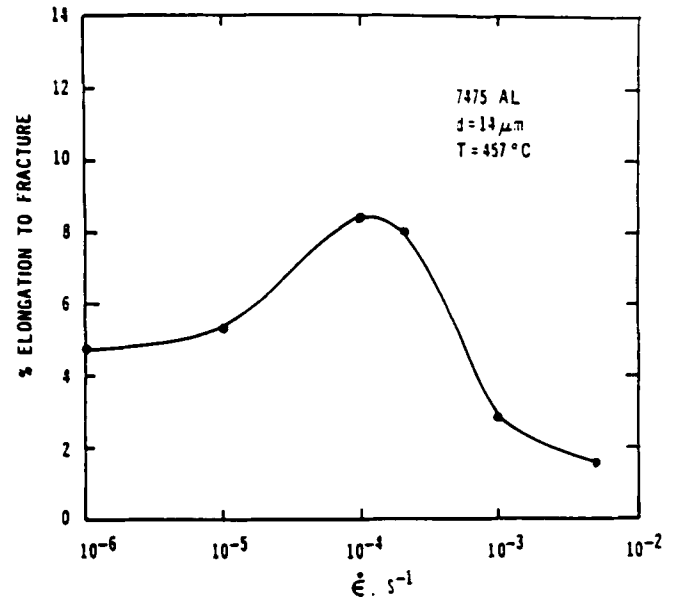
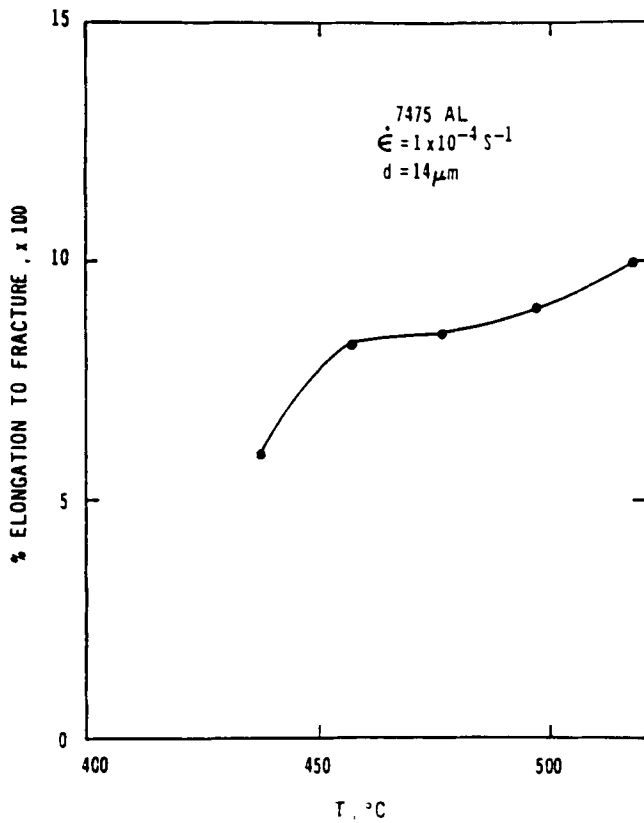


(a)



(b)

Fig. 6 Strain homogeneity along the gage section of specimens deformed to fracture at 457 °C (a) and 517 °C (b)



(b)

(a)

Fig. 7 Plot of elongation to fracture versus test temperature ($\dot{\epsilon} = 1 \times 10^{-4}/\text{s}$) (a) and strain rate ($T = 457 \text{ }^\circ\text{C}$) (b) for 7475 Al alloy

References

1. A.K. Mukherjee, in *Materials Science and Technology: A Comprehensive Treatment*, Vol 6, R.W. Cahn, P. Haasen, and E.J. Kramer, Ed., VCH Publishers, 1993, p 407
2. A.H. Chokshi, A.K. Mukherjee, and T.G. Langdon, *Mater. Sci. Eng. Rep.*, Vol R10, 1993, p 237
3. J.A. Wert, N.E. Paton, C.H. Hamilton, and M.W. Mahoney, *Metall. Trans. A*, Vol 12A, 1981, p 1265
4. M.W. Mahoney and C.H. Hamilton, "Superplastic Aluminum Evaluation," Report No. AFWAL-TR-81-3051, U.S. Air Force Flight Dynamics Laboratory (AFWAL/FIB), 1981
5. N.E. Paton and C.H. Hamilton, U.S. Patent 4,092,181, April 25, 1977
6. H.E. Adabbo, G.G. Doncel, O.A. Ruano, J.M. Belzunce, and O.D. Sherby, *J. Mater. Res.*, Vol 4, 1989, p 587
7. M.K. Rao and A.K. Mukherjee, *Scr. Metall.* Vol 20, 1986, p 411
8. R.K. Mahidhara, to be published
9. R.G. Fleck, G.J. Cocks, and D.M.R. Taplin, *Metall. Trans. A*, Vol 1A, 1970, p 3415
10. H. Ishikawa, D.G. Bhat, F.A. Mohamed, and T.G. Langdon, *Metall. Trans. A*, Vol 8A, 1977, p 523
11. F.A. Mohamed, M.M.I. Ahmed, and T.G. Langdon, *Metall. Trans. A*, Vol 8A, 1977, p 933
12. C.H. Hamilton, C.C. Bampton, and N.E. Paton, in *Superplastic Forming of Structural Alloys*, N.E. Paton and C.H. Hamilton, Ed., TMS-AIME, 1982, p 173